Limnol. Oceanogr., 56(4), 2011, 1399–1410
© 2011, by the American Society of Limnology and Oceanography, Inc.
doi:10.4319/lo.2011.56.4.1399

Diatom frustules show increased mechanical strength and altered valve morphology under iron limitation

Susanne Wilken,[a,b,c] Bernd Hoffmann,[d] Nils Hersch,[d] Norbert Kirchgessner,[d,e] Sabine Dieluweit,[d] Wolfgang Rubner,[d] Linn J. Hoffmann,[a,f] Rudolf Merkel,[d] and Ilka Peeken[a,g,h,*]

[a] Leibniz-Institute of Marine Sciences, Kiel, Germany
[b] Department of Aquatic Ecology, Netherlands Institute of Ecology, Wageningen, The Netherlands
[c] Aquatic Microbiology, Institute for Biodiversity and Ecosystem Dynamics, University of Amsterdam, Amsterdam, The Netherlands
[d] Institute of Complex Systems, ICS-7: Biomechanics, Forschungszentrum Jülich, Jülich, Germany
[e] Institute of Agricultural Sciences, Swiss Federal Institute of Technology Zürich, Zürich, Switzerland
[f] Department of Chemistry, University of Otago, Dunedin, New Zealand
[g] Alfred Wegener Institute of Polar and Marine Research, Bremerhaven, Germany
[h] MARUM - Center for Marine Environmental Sciences, University of Bremen, Bremen, Germany

Abstract

Iron limitation often results in increased cellular silica contents of diatoms, suggesting that diatoms grow thicker and possibly mechanically stronger frustules when limited. We performed stability measurements for six diatom species grown under iron-limitation and iron-sufficient conditions. Frustule strength increased in all species when grown under iron limitation, with this effect being statistically significant for four of them. Valve morphology and silica content of the pennate *Fragilariopsis kerguelensis* and the centric *Coscinodiscus wailesii* changed under iron limitation but only valve morphology changes were significant; *F. kerguelensis* grew thicker costae while *C. wailesii* had smaller pores, especially in the outer part of the valves. These morphological changes are clearly in agreement with increased mechanical strength. Increased cellular silica concentrations in diatoms grown under iron limitation do result in increased frustule strength, most likely improving their protection against grazers.

Diatoms account for 20–40% of the oceanic primary production (Nelson et al. 1995) and are major contributors to the carbon export to the deep ocean by the biological carbon pump (Buesseler 1998). In large parts of the ocean phytoplankton growth does not reach its full capacity despite high macronutrient concentrations. In these high-nutrient low-chlorophyll (HNLC) areas primary productivity is limited by the low availability of iron (Martin and Fitzwater 1988; Martin et al. 1990). Mesoscale in situ iron-enrichment experiments have successfully induced phytoplankton blooms that were mainly dominated by large or chain-forming diatoms (De Baar et al. 2005), demonstrating the key role of this group in primary production and potential carbon export in HNLC areas.

The phytoplankton blooms induced by iron addition have not always been followed by an increase in carbon export (Boyd et al. 2007) and food-web structure seems to play an important role in determining export production. Although some studies found the export to be dominated by sinking of phytoplankton detritus (Waite and Nodder 2001; Jackson et al. 2005) as consistent with the view that high-biomass waters export a significant fraction of the primary production directly as phytoplankton aggregates (Turner 2002), in other cases export was controlled by densely packed fecal pellets (Ebersbach and Trull 2008), demonstrating the role of mesozooplankton grazing in controlling and even enhancing carbon export. While grazing by herbivorous mesozooplankton can contribute to high export conditions through the production of fast-sinking fecal pellets, coprivorous mesozooplankton can also enhance remineralization by processing of fecal pellets within the upper mixed layer and, thereby, reduce the export into deeper waters (Wassmann 1998). The latter process might explain the 'high biomass, low export' conditions found during the Southern Ocean Iron Experiment (SOFeX) with a 10-fold increase in > 51-μm biomass after iron fertilization, albeit apparently no increase in particle export (Lam and Bishop 2007). For a better understanding of carbon export it is, therefore, crucial to understand the factors influencing zooplankton grazing rates in the ocean, especially on phytoplankton groups like diatoms that usually dominate export production.

Although resource competition has been traditionally regarded as the main factor shaping phytoplankton community composition, top-down factors like mortality due to grazing are also drivers of phytoplankton evolution and can determine community structure (Smetacek et al. 2004; Assmy et al. 2007). The silica frustules of diatoms can withstand strong forces and provide an effective mechanical protection against grazers, like copepods (Hamm et al. 2003), which often dominate the mesozooplankton community in the ocean (Voronina 1998). The strong mouthparts of copepods that feed on these well-protected diatoms seem to have coevolved with the frustules of their prey (Michels and Schnack-Schiel 2005), and heavily silicified, mechanically resistant species are typically an important component of the phytoplankton community in the Southern Ocean HNLC area (Assmy et al. 2007).

* Corresponding author: Ilka.Peeken@awi.de

Because iron limitation alters the elemental stoichiometry of diatoms showing an increase in Si : C and Si : N-ratios when grown under iron limitation (Hutchins and Bruland 1998; Takeda 1998; Franck et al. 2003) it has been predicted that iron-limited diatoms grow thicker shells (Boyle 1998). Although increased ratios of silica to other elements can also be caused by decreasing C- and N-quotas under iron limitation (Takeda 1998; Marchetti and Harrison 2007; Bucciarelli et al. 2010), iron-limited diatoms do indeed often show an increased cellular Si content (Takeda 1998; De La Rocha et al. 2000; Leynaert et al. 2004). The mechanism causing the increase in silica content during iron limitation is thought to be an indirect one. Silicate uptake does not take place constantly over the whole cell cycle, but is mainly confined to the gap 2 and mitosis (G2 + M) phase prior to building the new valves of the daughter cells (Brzezinski 1992). During iron limitation diatoms most likely arrest in this phase of the cell cycle, leading to a prolongation of the period of silicate uptake and, thereby, resulting in higher cellular silica contents (Martin-Jézéquel et al. 2000). Such a mechanism has been shown during growth limitation by other factors such as nitrogen, phosphorus, and light limitation (Claquin et al. 2002), and is likely to act in the same way during iron limitation. Increased silica content does not, therefore, seem to be a specific reaction to iron limitation. Clearly, an increased Si content might result in thicker frustules with a higher mechanical resistance, which in turn might influence their susceptibility to grazers.

Here, we investigated the effect of iron availability on the valve strength of 6 diatom species. We chose one pennate species, the heavily silicified, chain-forming *Fragilariopsis kerguelensis*, which often dominates the phytoplankton community in the Southern Ocean. Furthermore we studied five centric species: *Porosira pseudodelicatula* and *Thalassiosira tumida* (both species occurring in the Southern Ocean), and the cosmopolitan species *Thalassiosira rotula*, *Coscinodiscus granii*, and *Coscinodiscus wailesii*. For *F. kerguelensis* and the large centric *C. wailesii* we additionally investigated the effect of iron limitation on their valve morphology and silica content and found significant changes in pore size and frustule thickness.

Methods

Diatom strains and culture conditions—Cultures of *C. wailesii*, *C. granii*, and *T. rotula* were obtained from the Alfred Wegener Institute in Bremerhaven, Germany, and had been isolated from the North Sea. *P. pseudodelicatula* (CCMP 1550) and *T. tumida* (CCMP 1044) were obtained from the Provasoli-Guillard National Center for Culture of Marine Phytoplankton (CCMP). *F. kerguelensis* had been isolated during the iron-enrichment experiment EIFEX (Hoffmann et al. 2007).

The Antarctic diatoms *F. kerguelensis*, *T. tumida*, and *P. pseudodelicatula* were grown at 3°C and 30 μmol quanta m^{-2} s^{-1} with a light : dark cycle of 16 h : 8 h while the remaining cultures were grown at 18°C and 80 μmol quanta m^{-2} s^{-1} with a light : dark cycle of 12 h : 12 h. Light was provided by cool fluorescence tubes (Osram fluora L18 W/77 and Biolux 18 W/965). All phytoplankton cultures were grown in artificial seawater consisting of 400 mmol L^{-1} NaCl, 20 mmol L^{-1} $MgSO_4$, 7.5 mmol L^{-1} $CaCl_2$, 1.7 mmol L^{-1} KBr, 10 mmol L^{-1} KCl, 20 mmol L^{-1} $MgCl_2$, 2 mmol L^{-1} $NaHCO_3$, and 0.2 mmol L^{-1} H_3BO_3 with f/2 nutrient enrichment (Guillard and Ryther 1962). Deviating from the original f/2 media, twice the usual amount of Si was used (0.21 mmol L^{-1}) to prevent Si-limitation. For the iron-replete media, iron was added to a final concentration of 1 μmol L^{-1}; for the iron-limited conditions, no iron was added to the media. All other trace elements were kept at f/2 concentrations. Care was taken to prevent contamination with iron. All material coming into contact with the media or the cultures was cleaned with hydrochloric acid before usage. Cultures and media were handled in a laminar flow hood using trace-metal clean techniques.

To establish iron-limited cultures from the iron-replete ones, the cultures were transferred into iron-free medium. For this, the cells were left to sink down overnight; the medium was removed and replaced by iron-free medium. This procedure was repeated five times and cultures were left to grow into iron limitation. As an indicator for iron limitation the maximum photochemical yield (Φ_M) was measured in both iron-replete and -deplete cultures using a Phyto-PAM fluorometer according to Kolbowski and Schreiber (1995). Samples were dark-adapted for 10 min prior to the measurements. As soon as Φ_M dropped below a value of 0.3, cultures were considered to be limited. From these stock cultures triplicate cultures were established for both nonlimited and iron-limited conditions by transferring stock cultures into fresh medium with and without iron, respectively. Samples were taken during exponential growth after incubation for 10–11 d and processed as described below. Φ_M was measured prior to sampling to confirm iron limitation in iron-deplete cultures and assure that iron-replete cultures did not run into limitation.

Measurements of mechanical resistance—Measurements of mechanical resistance were performed under a microscope (Axiovert 200; Zeiss, Germany) using calibrated glass needles as described in Hamm et al. (2003). The needles were pulled using a Flaming–Brown Micropipette Puller (Model P-97; Sutter Instrument). For calibration, the needles were pressed against accurate scales (LabStyle 204, Mettler Toledo) by moving the base of the needle in 5-μm intervals using a micromanipulator (Narishige International). The acting forces were calculated from the weight reading of the scale and showed a linear relationship to the distance covered by the needle. For the actual measurements of mechanical resistance, cells were pressed against the edge of a microscope slide glued upon a cover glass, again by moving the needle in 5-μm intervals. The distance covered by the needle until the cell broke was noted and the corresponding force calculated. The resistance measurements were performed in three different positions as depicted in Fig. 1. In position A, the force was applied onto the girdle-band region; in position B, the force was also applied onto the girdle-band region, albeit this time perpendicular to the plane of the valves. In position C and

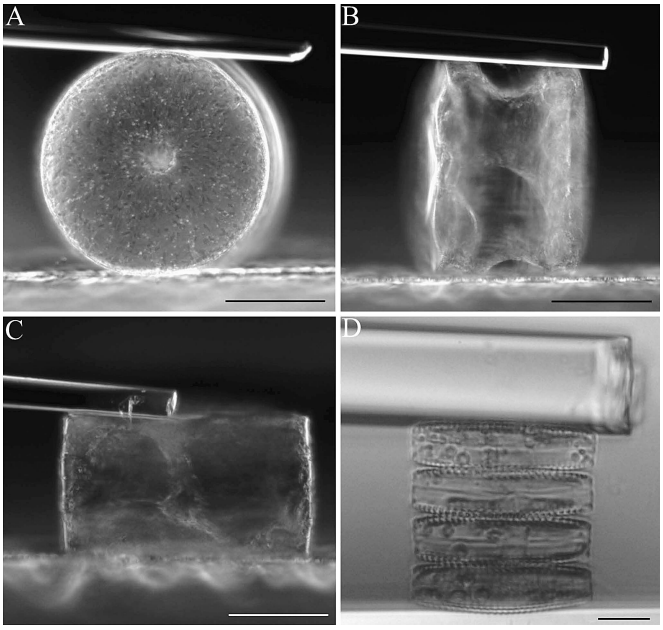

Fig. 1. Positions in which the forces were applied for the stability measurements shown for (A–C) *C. wailesii*, and (D) *F. kerguelensis*. In position A, forces were applied onto the girdle-band region; in position B, forces were applied on the edges of the valves perpendicular to the girdle bands; and in position C and D, forces were applied onto the center of the valves. In position D, forces were applied onto multiple cells in a chain. Scale bars represent 100 μm in panels A–C and 10 μm in panel D.

D, the force was applied onto the center of the valves. Position D refers to measurements of *F. kerguelensis* where the force was applied on multiple cells in a chain. For each treatment and position between 7 and 19 stability measurements were performed. Unfortunately, the resistance measurements could not be reliably performed in all positions for all species, because chain formation prevented the positioning and especially the more fragile species were very prone to damage during turning.

Because the force that can be applied with a certain needle strongly depends on its diameter and because the mechanical resistance of the species investigated differed widely, different needles had to be used for different species. This and the dissimilarity in cell size between the species might lead to differences in contact areas between the needles and the cells and, therefore, to altered pressures applied to the cells. However, care was taken to use the same needle for both iron treatments within one species to assure comparability. For a better comparison between different species, pressures were calculated for the iron-replete treatments based on the measured forces and an estimated contact area.

Investigation of valve morphology—The valve morphology of *F. kerguelensis* was investigated by scanning electron microscopy (SEM) and confocal laser scanning microscopy (LSM) while *C. wailesii* was analyzed only by LSM. To remove organic material from the silica frustules of *F. kerguelensis* for SEM analyses, 15 mL 35% H_2O_2 were added to 5 mL of culture and heated to 60°C for 15 min. The mixture was diluted with 0.5 liter of water and the cells were filtered onto polycarbonate filters (0.2-μm pore width). Filters were dried at 50°C overnight. Small pieces were cut from the filters, sputtered with a gold palladium mixture, and viewed and photographed in a SEM (CamScan-CS-44, CamScan). Apical length, transapical width, width of the costae, and distances between the costae were measured for 13 cells of both treatments using the image analysis software ImageJ. Aspect ratios were calculated by dividing the apical length by the transapical width (Marchetti and Harrison 2007) to give an indication for the valve shape. As a measure for the density of the costae over the length of the cell, both number of costae/10 μm and the F^* values (Cortese and Gersonde 2007) are recorded. F^* is calculated as

$$F* = \frac{\text{apical length} \times \text{length of 5 costae}}{\text{transapical width}}$$

It gives the density of costae weighted by valve length and width and can, therefore, be regarded as a general shape and costae density index with lower F^* values corresponding to denser costae and more mechanically resistant valves (Cortese and Gersonde 2007). Furthermore, for valve morphology characterization of *F. kerguelensis* diatoms, LSM images (LSM 510meta, Zeiss) were taken. For this purpose, diatoms were washed in phosphate-buffered saline (PBS) and subsequently analyzed in phase contrast using a 488-nm argon-ion laser.

Due to the bent shape of *C. wailesii* valves, SEM did not give sharp images of whole valves and, therefore, z-stacks were taken on the LSM in fluorescence and subsequently used for image processing (*see* below). For this purpose, diatoms were stained with rhodamine 123 (R123; Invitrogen) as described in Brzezinski and Conley (1994). Because this fluorescent dye is only incorporated into newly formed silica structures, the cultures were grown with 2 μg mL^{-1} R123 for 10 d. To remove unbound dye prior to analysis, cells were washed by centrifuging 1.5 mL of the culture, rejecting the supernatant, and resuspending the pellet in 1.5 mL PBS. This procedure was repeated six times. At the end, z-stacks were taken for 8 cells/treatment, using a Plan-Apochromat 63X/1.4 oil immersion lens. Illumination was performed using the 488-nm argon-ion laser line and emitted light was detected with a 505–550-nm band-pass filter. For all scans, microscope settings were kept stable.

Image processing—For reconstruction of a single focused image of the bent surface of *C. wailesii*, the z-stacks were rank-value filtered (Jähne 2005). That is, at each position, the slices were sorted according to brightness and the grey value of the nth slice was taken for reconstruction. n was chosen interactively. The resulting single image was median-filtered using a 5×5 region of interest. Uneven illumination of the reconstructed image was removed by dividing it with an extremely smoothed version of itself. This resulted in images as shown in Fig. 2A. The distributions of brightness of these images were bimodal. Pixels belonging to the brighter peak were selected as structure by threshold segmentation. Subsequently, all objects smaller than 0.175 μm^2 were removed (Fig. 2B).

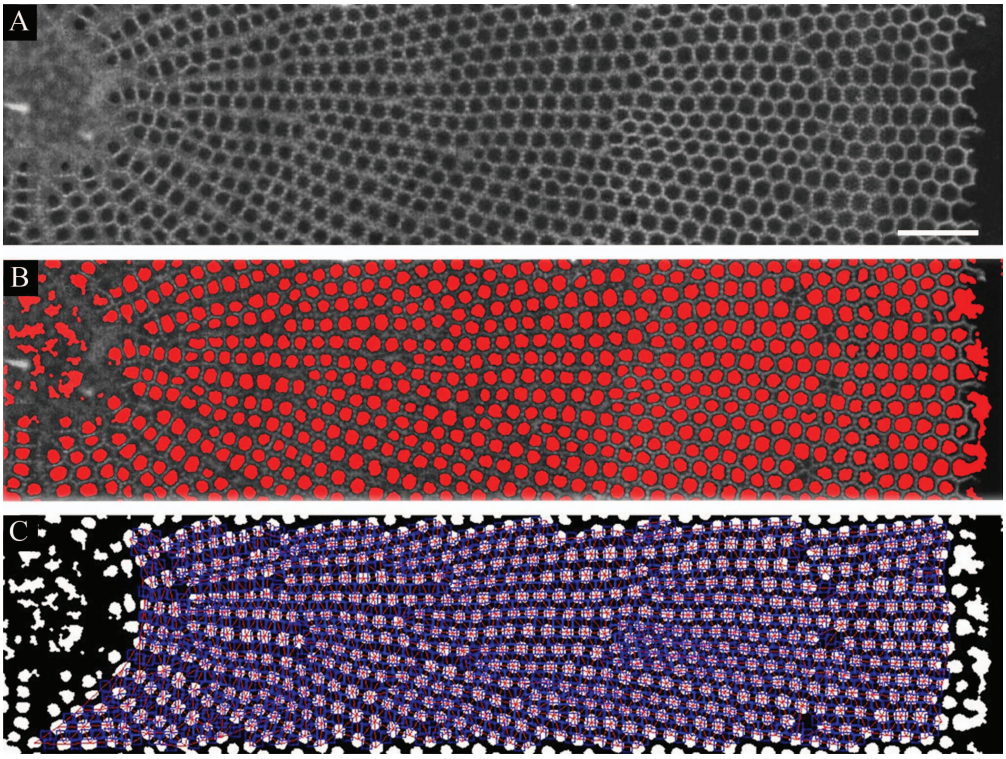

Fig. 2. Image processing of *C. wailesii* and valve morphological analyses. (A) z-stacks of *C. wailesii* LSM images were reconstructed to one image and corrected for varying brightness. Scale bar represents 10 μm. Subsequently, (B) structures were segmented and the area of pores was determined (red areas). (C) Segmented images were the basis of all subsequent analyses.

On such reconstructed and segmented micrographs all valve morphology measurements were performed (Fig. 2C). To determine the area of pores, all pixels (0.05 $\times$ 0.05 μm) within were counted. For calculating the area of unit cells (i.e., the area of pores with the surrounding silica wall), centroid positions of all pores were determined. In a next step centroid positions were connected by triangulation according to Barber et al. (1996), resulting in an irregular hexagonal mesh of all centroids. Because the number of triangles in such a mesh is twice the number of nodes, we doubled the average area of triangles to get the area of unit cells. The width of the walls was determined along the triangulation by calculating the Euclidean distance map (Russ 2002) of the pores.

On the much smoother *F. kerguelensis*, focused micrographs could be taken directly. In a first step, these micrographs were median-filtered and corrected for uneven illumination as described above. However, due to the different contrast of pores in this species we had to proceed differently from here on. In essence we exploited the fact that gray values changed strongly at pore boundaries. Hence boundaries could be found by an energy-minimizing active contour technique (i.e., the snake algorithm; Amini et al. 1990). Here we used the gray value gradient as energy term. Because this algorithm needs an initialization, we extracted estimates of the pore boundaries by calculating the z-score (Jähne 2005) of the images (91 $\times$ 91 square regions) and using this z-score image for threshold segmentation. This yielded a first estimate of the pore boundaries. Subsequently, short segments, nonclosing lines and image edges were discarded. The remaining boundaries were used as starting lines for the snake algorithm. Finally pores were grouped according to the stria they appeared in. All geometrical parameters were calculated from these grouped and smooth boundary lines as shown in Fig. 3.

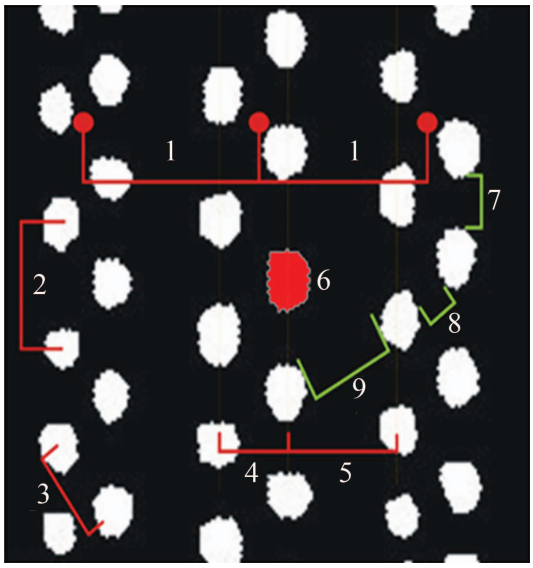

Fig. 3. Morphological valve characterization of *F. kerguelensis*. Values for the distances and areas indicated by numbers in the filtered and segmented image are given in Table 3.

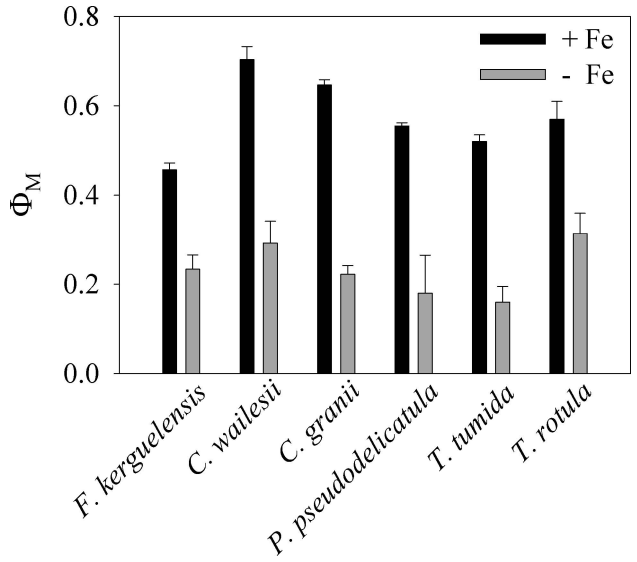

Fig. 4. Maximum photochemical yield of iron-replete and -deplete cultures at the end of the experimental incubations. Error bars indicate standard deviation.

Cellular silica content—For the determination of the particulate silica concentration, samples were filtered onto cellulose-acetate filters and stored at −20°C until further processing. Samples were digested by incubation in 0.1 mol L^{-1} sodium hydroxide at 85°C for 2 h. Measurement of biogenic silica was performed according to Hansen and Koroleff (1999). Samples for determination of cell numbers were fixed with Lugol's Iodine Solution and stored at 4°C until microscope counting.

Statistical analysis—When data were normally distributed and variances were homogenous, Student's *t*-test was used for comparisons between iron-replete and -deplete treatments. Only the data of costae width in *F. kerguelensis* were not normally distributed and, therefore, the nonparametric Mann–Whitney *U*-test was used instead. The stability measurements for *C. wailesii* and *P. pseudodelicatula* were analyzed by a two-factorial analysis of variance followed by a Tukey post hoc comparison to distinguish between the effects of iron limitation and position of stability measurement. All statistical analyses were performed using the STATISTICA 8 software (StatSoft).

Results

All six diatom species investigated showed a decrease in maximum photochemical yield by 50% to 65% when grown in iron-deplete medium as compared to iron-replete conditions (Fig. 4); even though we did not measure dissolved iron concentrations in the media, we can, therefore, be confident that the cultures were indeed limited by iron availability.

Measurements of mechanical resistance—The mechanical resistance of the six diatom species investigated differed substantially. The forces they were able to withstand ranged from about 10 μN for the two rather small *Thalassiosira* species up to 1300 μN for the large *C. wailesii* under iron limitation (Fig. 5). The rather small but heavily silicified *F. kerguelensis* possessed very strong valves with yield forces of 150 to 250 μN (Fig. 5B). When the differences in contact areas between needle and cells were taken into account to calculate the pressure the frustules could withstand, the variation between species was lower (Table 1). For the larger contact areas, especially in the case of *C. wailesii* and *C. granii*, an even distribution of the force over the entire contact area cannot be assured; therefore, the presented pressures are only a rough estimate and most likely underestimate the pressures that the large species are able to withstand. Nevertheless, the exceptional strength of *F. kerguelensis* frustules became more evident. While the five centric species were able to withstand pressures between 0.07 Nmm^{-2} and 0.17 Nmm^{-2} under iron-replete conditions and between 0.09 Nmm^{-2} and 0.41 Nmm^{-2} under iron limitation, the pressure of 1.26 Nmm^{-2} and 2.03 Nmm^{-2} needed to break the *F. kerguelensis* frustules was about an order of magnitude higher (Table 1).

All six diatom species investigated showed the same trend toward more stable valves when grown under iron limitation. This difference was significant for *P. pseudodelicatula* ($F_{1,57} = 55.35$; $p < 0.001$), *F. kerguelensis* (*t*-test = −5.09; df = 23; $p < 0.001$), *C. wailesii* ($F_{1,69} = 119.45$; $p < 0.001$), and *C. granii* (*t*-test = −4.21; df = 32; $p < 0.001$) with a 1.5-fold to 3-fold increase in their valve strength for cells grown under iron limitation. While for *P. pseudodelicatula*, iron limitation caused increased valve strength in all three positions of the measurements (Fig. 5A), the effect on valve strength of *C. wailesii* depended on the position in which the force was applied. When the force was directly applied to the valves in position B, iron limitation resulted in a three-fold increase in mechanical resistance, whereas the difference in forces needed to break the cells when applied on the girdle bands in position A was not significant (Fig. 5D).

In SEM and LSM micrographs, neither *F. kerguelensis* nor *C. wailesii* showed a change in cell size due to iron limitation. Also the aspect ratio of *F. kerguelensis* cells and the density of their costae, measured as the number of costae over a length of 10 μm or as the *F** value, did not change significantly (Table 2). However, SEM images of *F. kerguelensis* showed a pronounced and significant change in valve morphology, with cells grown under iron limitation having 50% thicker costae than cells grown under iron-replete conditions (Table 2; Fig. 6A,B). Quantitative analyses of LSM images of *F. kerguelensis* valves also revealed statistically significant differences ($p = 0.01$). Here, pore sizes as well as their distances in all relevant directions and the distances and widths of the striae were analyzed (Figs. 3; 6C,D). In summary, pores were significantly larger but fewer in *F. kerguelensis* when grown under iron limitation (Table 3). Their mutual distances increased significantly and only the distance between the pores of the two rows within a multiseriate stria was not significantly changed (parameter No. 4 in Table 3). Furthermore, LSM measurements revealed a significantly enlarged striae widths (Table 3; Fig. 6C,D).

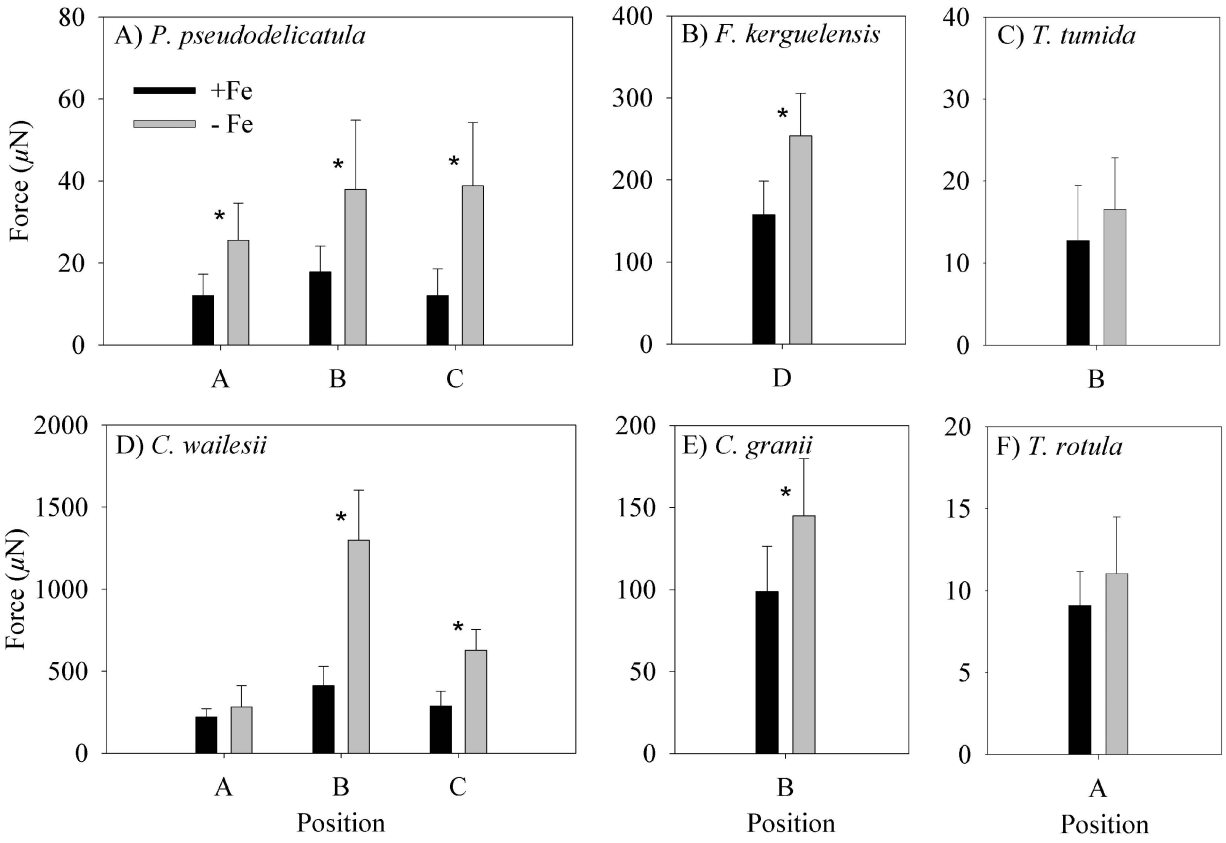

Fig. 5. Forces necessary to break the diatom frustules of (A) *P. pseudodelicatula*, (B) *F. kerguelensis*, (C) *T. tumida*, (D) *C. wailesii*, (E) *C. granii*, and (F) *T. rotula*. The position in which the force was applied is indicated on the x-axis. Error bars indicate standard deviation. Significant differences ($p < 0.05$) between iron-replete and iron-deplete treatments are indicated by an asterisk.

Similar results were also found for *C. wailesii*. Here, quantitative analyses of LSM images revealed significantly reduced pore sizes for diatoms grown under iron-limited conditions (Fig. 7A). These differences are present over the whole radius of the diatoms, with pore sizes of ~ 0.6 μm^2 close to the center of the valve to 1.1 μm^2 at the edge for depleted diatoms, as compared to 0.9-μm^2 to 1.8-μm^2 pore size close to the center and at the edge of the valve, respectively, in iron-replete cells. Interestingly, while silica structures around the pores get thinner with increasing radius for diatoms grown under iron-replete conditions, iron-limited conditions result in a similar thickness in the center of the diatoms that stays almost stable over the whole radius of the shell (Fig. 7B). For the pore center to center distance under iron-replete conditions, the effect of thinner silica structures is compensated by the enlarged size of the pores resulting in enlarged distances of pore centers (Fig. 7C). This also explains why the unit cell area (i.e., the area of the pore together with the surrounding silica structure) is enlarged for *C. wailesii* grown under iron-replete conditions. However, this increase in unit cell size is mainly accounted for by pore growth and is, therefore, the most likely reason for diminished stability (Fig. 7D).

The cellular silica content of both *F. kerguelensis* and *C. wailesii* showed a trend toward a higher silica content under iron limitation (Fig. 8). The amount of silica per cell

Table 1. Estimated contact area between the needle and the cell during stability measurements, measured forces, and calculated pressure necessary to break the valves. For *C. wailesii* and *P. pseudodelicatula*, presented values are means of the three different positions for stability measurements.

Species	Contact area (μm^2)	Force (μN) +Fe	Force (μN) −Fe	Pressure (N mm^{-2}) +Fe	Pressure (N mm^{-2}) −Fe
F. kerguelensis	125	158	254	1.26	2.03
P. pseudodelicatula	125	14	34	0.11	0.27
C. wailesii	1800	306	736	0.17	0.41
C. granii	1500	99	145	0.07	0.10
T. rotula	125	9	11	0.07	0.09
T. tumida	125	13	17	0.10	0.14

Table 2. Cell morphology of *F. kerguelensis* cells grown with and without iron as assessed by SEM. Standard deviations are given in parenthesis. Differences were tested using the Student's *t*-test except for the nonnormally distributed data of costae width where the Mann–Whitney *U*-test was used instead. In all cases $n = 13$.

	With Fe	Without Fe	Statistic	*p*
Apical length (μm)	36.55(3.50)	37.09(4.51)	$t_{23} = -0.34$	0.74
Transapical width (μm)	10.02(0.56)	9.75(0.59)	$t_{23} = 1.17$	0.25
Aspect ratio	3.66(0.42)	3.82(0.58)	$t_{23} = -0.81$	0.43
Costae 10 μm^{-1}	7.67(0.64)	7.22(0.51)	$t_{23} = 1.93$	0.07
*F**	24.05(3.56)	26.67(5.07)	$t_{23} = -1.51$	0.15
Costae width (μm)	0.21(0.03)	0.30(0.06)	$U_{23} = -3.79$	<0.001

increased by a factor of 1.21 for *C. wailesii* and 1.43 for *F. kerguelensis*, respectively; however, for both species this difference was not significant.

Discussion

Mechanical resistance of diatom frustules—Diatoms possess strong silica frustules offering an effective mechanical protection (Hamm et al. 2003). The forces needed to crack diatom frustules varied considerably between the species investigated in our experiments. The large *C. wailesii* and the smaller but heavily silicified *F. kerguelensis* were able to withstand strong forces, whereas the yield forces of the smaller *Thalassiosira* species were ~ one order of magnitude lower. The yield forces of ~ 100 μN measured for *C. granii* compare well with those reported by Hamm et al. (2003), while those of *F. kerguelensis* are slightly lower in our study. Iron limitation induced an up to three-fold increase in valve strength, with the effect being significant for four of the six species investigated. Hence, an increase in valve strength under iron limitation seems to be a general trend in the diatoms examined. The strongest effect on mechanical resistance was observed for those species already possessing a higher mechanical strength under nonlimiting conditions, while the effect on the smaller and weakly silicified *Thalassiosira* species was not significant.

In contrast to *P. pseudodelicatula*, for *C. wailesii* the increase in mechanical resistance under iron limitation depended on the position in which the force was applied (Fig. 3). Apparently, only the valves became stronger and not the girdle-band region. A possible explanation might be that the formation of girdle bands is not confined to the G2 + M phase of the cell cycle, but might also take place during the G1 phase (Schmid and Volcani 1983). Therefore, if the silica content increases due to an elongation of the G2 + M phase during iron limitation, iron deficiency could have a very different effect on girdle bands and valves. Alternatively, the disconnection of girdle bands might have contributed to cells breaking. Not in all cases were silica structures of the girdle bands actually broken; some of them remained intact while disconnecting, causing the cell to open without breaking of the silica structures. The connection of the girdle bands might be the weakest part of the diatom cell wall and is apparently not strengthened by the increased silica content in *C. wailesii*.

Silica content and morphology—We did not observe any differences in cell size between the two iron treatments for the two species *F. kerguelensis* and *C. wailesii* and, therefore, did not normalize the silica content to biovolume or cell surface area. The constancy of cell size was to be expected considering the short time scale of our experiments, and is consistent with the results of Timmermans et al. (2004) and Hoffmann et al. (2007) for *F. kerguelensis*.

The cellular biogenic silica content of diatoms has been shown to increase from 1.4-fold for *T. weissflogii* (De La Rocha et al. 2000) up to 4-fold for *Cylindrotheca fusiformis* during iron limitation, when normalized to biovolume (Leynaert et al. 2004). The observed increases in cellular silica content of *F. kerguelensis* and *C. wailesii* were in the lower range of data reported in the literature and were not significant. Nevertheless, the increase by a factor of 1.4

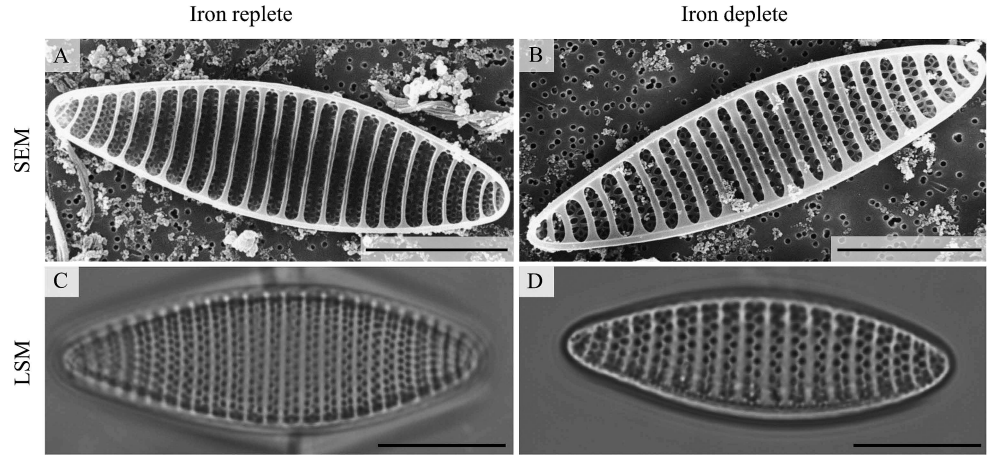

Fig. 6. Scanning electron microscopy (SEM) images of *F. kerguelensis* valves grown under (A) iron-replete and (B) -deplete conditions. Laser-scanning micrographs of *F. kerguelensis* grown under (C) iron-replete and (D) -deplete conditions. Scale bars represent 10 μm.

Table 3. Cell morphology of *F. kerguelensis* cells grown with and without iron as assessed by Laser Scanning Microscopy. Number denotation: (1) width of striae; (2) distance between pore centers within a line; (3) distance of pore centers on different lines in a multiseriate stria; (4) distance between both lines in a multiseriate stria; (5) distance between closest lines in adjacent striae; (6) area of pore; (7) width of ribs between pores within a line; (8) width of ribs between pores on different lines within a multiseriate stria; (9) widths of ribs between different striae. Numbers in brackets = standard deviation. Number of analyzed structural features = *n*. Statistical tests were performed with a *p*-value of 0.05.

Parameter	With Fe	*n*	Without Fe	*n*	Significance
1 (μm)	1.62(0.09)	42	1.86(0.16)	47	+
2 (μm)	0.74(0.11)	831	1.03(0.46)	553	+
3 (μm)	0.79(0.14)	850	0.85(0.11)	608	+
4 (μm)	0.72(0.17)	52	0.68(0.12)	58	−
5 (μm)	0.89(0.10)	42	1.18(0.11)	47	+
6 (μm^2)	0.09(0.02)	938	0.14(0.04)	681	+
7 (μm)	0.37(0.09)	831	0.58(0.23)	553	+
8 (μm)	0.35(0.14)	850	0.31(0.10)	608	+
9 (μm)	0.59(0.12)	743	0.77(0.12)	518	+

under iron limitation in *F. kerguelensis* is within the same range as reported for the same strain by Hoffmann et al. (2007), and is high enough to account for the observed change in the width of the costae. Because the costae help to absorb the stress from the more fragile areas in between (Hamm et al. 2003), increasing their thickness might be the most efficient mechanism to increase overall frustule strength. A similar effect could theoretically be reached by a higher costae density over the cell length as measured by the *F** value or the number of costae/10 μm. A variation of *F** values in *F. kerguelensis* valves from sediment cores of Atlantic and Pacific sectors of the Southern Ocean has been reported by Cortese and Gersonde (2007) and *F** values correlated strongly with net primary production, which in turn largely depends on iron availability (Marchetti and Cassar 2009). However, we did not observe any effect on costae density, probably because the change in cellular morphology over the course of our short-term experiments was less pronounced than in natural systems, where diatoms are subjected to iron limitation for long periods and where not only physiological changes but also ecological and evolutionary factors play a role.

Comparable to the situation in *F. kerguelensis*, *C. wailesii* also showed clear altered valve morphology, despite only minor changes in the cellular silica content. While *F. kerguelensis* formed fewer but larger pores under iron limitation, pore sizes of *C. wailesii* decreased, especially in the outer area of the valves. This indicates an increased silicification in the stronger areas of the valve in between the pores, which probably causes the higher valve stability. However, the valves of *C. wailesii* possess a complex honeycomb-like structure consisting of hexagonal areolae, which are confined by silica plates both toward the inside and the outside of the cell. While the pores at the inner side of the valve are closed by a thin silica layer that is again perforated by several smaller pores, the pores at the outer side of the valves are open and these are the ones we measured. This known architecture and its mechanical integrity was verified by scanning force microscopy (data not shown). While a decreased size of these pores is likely to increase the overall mechanical resistance of the valve, there remain several possible alterations of the complex valve structure that escape our analysis because they would require an even higher resolution than can be achieved by LSM.

For both species investigated the small increase in cellular silica content was strong enough to cause a clear change in valve morphology, resulting in a substantially increased mechanical resistance. Hence, for those species showing a stronger response in their cellular silica content the effect of iron limitation on the strength of diatom valves can be expected to be even stronger than the up to three-fold increase observed in our study.

The potential to increase the mechanical protection under iron limitation requires saturating dissolved concentrations of silicic acid for silicate uptake, because a silicic acid limitation causes the cellular silica content of diatoms to decrease (Martin-Jézéquel et al. 2000). In most HNLC areas, silicic acid concentrations are high enough to allow diatoms to have a high silica content while iron-limited. However, in the Southern Ocean north of the Antarctic Polar Front Zone and in the equatorial Pacific, for example, silicic acid concentrations are low and diatoms can be co-limited by silicic acid (Coale et al. 2004; Brzezinski et al. 2011). In this case they are not able to increase their mechanical protection even if low iron concentrations limit the primary productivity. If, on the other hand, silicic acid limitation only starts playing a role after diatoms are relieved from iron limitation, the decrease in mechanical protection during bloom formation can be expected to be even stronger as both the relief from iron limitation and the onset of silicic acid limitation lead to weakened diatom frustules (Hoffmann et al. 2008).

Implications for grazers—The strong silica frustules of diatoms and the mandibles of copepods lined with silica-reinforced teeth have probably coevolved. In such an evolutionary arms race there will not be a clear winner that is protected against all predators or able to handle all prey defense systems. On the contrary a prey species can only be protected against a fraction of its potential predators, but a small improvement in its defense system, like an increase in valve strength as observed during iron limitation, might already significantly increase this fraction. Because we are not aware of any study determining copepod bite forces or the mechanical strength of their mandibles, the effect of an

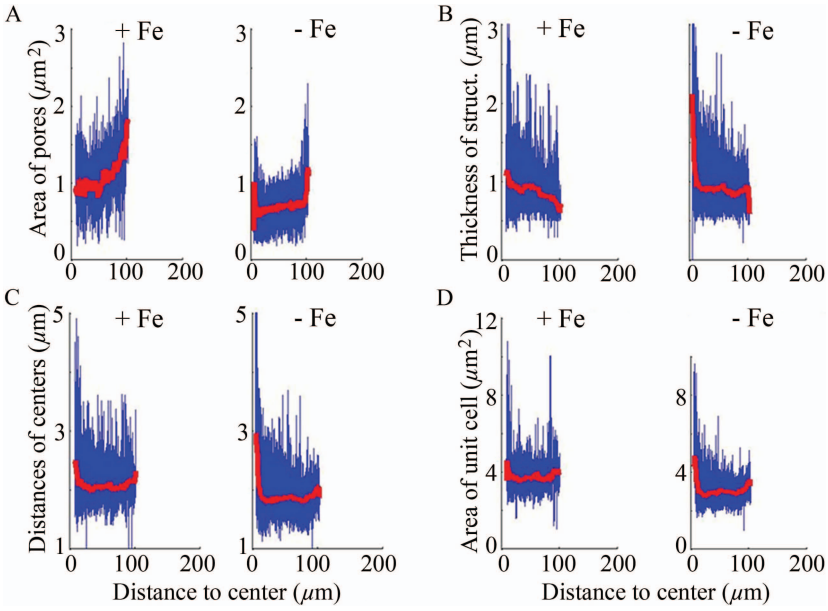

Fig. 7. *C. wailesii* (A) pore areas (n = 2418 analyzed structural features for +Fe, 3909 for −Fe), (B) thickness of silica structures around the pores (n = 6579 for +Fe, 10,896 for −Fe), (C) the distances from pore center to center (n = 6579 for +Fe, 10,892 for −Fe; red lines in Fig. 2C), and (D) the area of unit cells (n = 4012 for +Fe, 6702 for −Fe; blue lines in Fig. 2C). Red lines express mean values. Distributions for replete (+Fe) and deplete (−Fe) cells are in all cases significantly different (p = 0.05).

increased mechanical strength of diatoms is difficult to assess. Hamm et al. (2003) estimated that a predator needs to have muscle strands with a minimal diameter of 50 μm in order to be able to break *F. kerguelensis* cells. This criterion would only be met by large copepods and euphausids, while the strong shells protect *F. kerguelensis* against grazing by smaller copepods. An increase in valve strength of *F. kerguelensis* due to iron limitation would most likely further reduce the spectrum of potential predators to only the largest ones. In addition to the need for strong muscles to exert high forces, the mandibles of predator species must possess a higher mechanical strength than the diatoms they

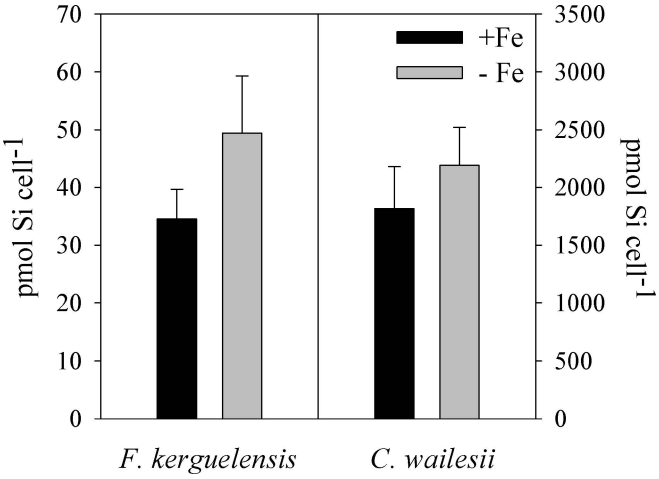

Fig. 8. Cellular silica content of *F. kerguelensis* and *C. wailesii* grown under iron-replete and -deplete conditions. Error bars indicate standard deviation.

are crushing. Miller et al. (1980) estimated the content of silica in the teeth of an adult *Acartia tonsa* to be 110 pmol. Considering the cellular Si content of *F. kerguelensis* and *C. wailesii* of 30–50 pmol and 1700–2100 pmol, respectively, it seems plausible that those shells provide an effective protection and a further increase in the mechanical strength might severely affect copepod grazers.

While it is plausible that an increased mechanical protection of diatoms has an effect on copepods and decreases the range of potential grazers, it is difficult to assess the effect on ingestion and growth rates of those grazers. A better mechanical protection could decrease copepod ingestion rates by increasing the handling time. But even after ingestion some species, like the well-protected *F. kerguelensis* and several *Thalassiosira* species, can remain intact during copepod gut passage (Kruse et al. 2009), indicating that a fraction of the ingested food cannot be assimilated by the grazers. An increase of this fraction can potentially cause lowered growth rates. Furthermore, because copepods are able to feed very selectively, they might also switch to other prey items as a response to an altered mechanical protection of diatoms. During several in situ iron fertilization experiments, copepod abundances and ingestion rates increased in the course of the bloom development (Rollwagen Bollens and Landry 2000; Zeldis 2001; Schultes et al. 2006) and Schultes et al. (2006) also reported a switch in dietary preferences of *Calanus simillimus* and *Rhincalanus gigas* from a preferred ingestion of ciliates toward diatoms in the fertilized patch. However, the differences between blooms and HNLC conditions are huge, and the effect of decreased mechanical protection cannot be separated from the effects of increased food

concentration and altered species composition. Furthermore, a weakened mechanical defense during bloom conditions might be compensated for by an improved chemical defense. For example the production of the toxin domoic acid by *Pseudonitzschia* species or of aldehydes that negatively affect the reproductive success of copepods would be most effective at high bloom abundances (Ianora et al. 2003).

In contrast to copepod grazers, euphausids filter water parcels through sieve-like maxillipedes and crush the ingested food in a strong gizzard. They are not likely to be deterred by increased valve strength and iron limitation will probably affect them most through altered phytoplankton abundance rather than through altered mechanical protection.

In addition to mesozooplankton grazers, microzooplankton grazing can also significantly contribute to diatom loss rates. In particular dinoflagellates are able to efficiently graze on large and chain-forming diatoms and this group was controlling the iron-induced diatom bloom during the Subarctic iron Enrichment for Ecosystem Dynamics Study (SEEDS) in the western subarctic Pacific (Saito et al. 2005). However, dinoflagellates are not crushing the entire frustule like copepods do. Some species are sucking the cell content, leaving the empty and almost intact shell behind, while others can ingest and digest whole cells without breaking the frustule first. It is, therefore, questionable whether an increased mechanical strength would improve the protection against dinoflagellate grazing. An altered mechanical resistance of diatoms might, therefore, influence different groups of grazers differently and potentially lead to a shift in zooplankton community composition.

Evolutionary ecology—Smetacek et al. (2004) argue that not only resource competition and selection for fast growth rates as present during the development of blooms, but also the mortality environment, shape phytoplankton evolution. Grazing pressure generally increases with decreasing food supply, implying that it is highest during HNLC conditions. This pattern has been confirmed by Schultes et al. (2006) for copepod grazing during the iron fertilization experiment EisenEx carried out in the Atlantic Sector of the Southern Ocean. Hence, defense against grazers becomes more important during conditions of resource limitation with phytoplankton growth rates being low. Because iron limitation characterizes HNLC conditions, well-protected diatoms such as the heavily silicified Southern Ocean species *F. kerguelensis* have a selective advantage in these areas, whereas fast-growing species are favored during blooms. These differences in selective pressure are reflected in a wide range of life-cycle strategies of phytoplankton, ranging from fast-growing, heavily grazed species to slow-growing, and well-defended ones. In our study these two extremes are represented by the cosmopolitan species *T. rotula* typically occurring in blooms and the heavily silicified *F. kerguelensis*, which is able to stand 18 times higher pressures than *T. rotula*. However, our results suggest that the position of a single species on this scale is not a fixed one, but that mechanical protection against grazers can be varied substantially depending on growth conditions. The degree of protection is increased during unfavorable growth conditions such as iron limitation, probably enabling the population to maintain positive net growth rates even though gross growth rates are low. Furthermore, the silica content of diatoms can also increase in response to the presence of copepod grazers (Pondaven et al. 2007), suggesting that diatoms increase the mechanical resistance of their frustules as an inducible defense. Because mesozooplankton grazing plays a key role in determining carbon export into the deep ocean, understanding the factors influencing grazing rates are crucial for the understanding of variations in export production. Here we show that iron limitation causes not only an increase in cellular silica content, but also an increase in the mechanical strength of diatom frustules, improving their mechanical protection against mesozooplankton grazers like copepods. Clearly, the effect of the improved defense on grazer growth and ingestion rates, and the role of this effect compared to the differences in food abundance and species composition between bloom and nonbloom situations, need to be further elucidated.

Acknowledgments

We thank J. Lezius for help with scanning electron microscopy (SEM). The SEM pictures have been made at the Laboratory for Scanning Electron Microscopy, Department of Geology at the Christian Albrechts University Kiel (CAU-Kiel). We thank two anonymous reviewers for their helpful comments on an earlier version of the manuscript. This research was funded by the German Research Foundation (DFG) grant PE_565_5 awarded to I. Peeken.

References

Amini, A. A., T. E. Weymouth, and R. C. Jain. 1990. Using dynamic programming for solving variational problems in Vision. IEEE Trans. Pattern Anal. Machine Intell. **12:** 855–867, doi:10.1109/34.57681

Assmy, P., J. Henjes, C. Klaas, and V. Smetacek. 2007. Mechanisms determining species dominance in a phytoplankton bloom induced by the iron fertilization experiment EisenEx in the Southern Ocean. Deep-Sea Res. Part I **54:** 340–362, doi:10.1016/j.dsr.2006.12.005

Barber, C. B., D. P. Dobkin, and H. Huhdanpaa. 1996. The quickhull algorithm for convex hulls. ACM Trans. Math. Software (TOMS) **22:** 469–483, doi:10.1145/235815.235821

Boyd, P. W., and others. 2007. Mesoscale iron enrichment experiments 1993–2005: Synthesis and future directions. Science **315:** 612–617, doi:10.1126/science.1131669

Boyle, E. 1998. Pumping iron makes thinner diatoms. Nature **393:** 733–734, doi:10.1038/31585

Brzezinski, M. A. 1992. Cell-cycle effects on the kinetics of silicic acid uptake and resource competition among diatoms. J. Plankton Res. **14:** 1511–1539, doi:10.1093/plankt/14.11.1511

———, and D. J. Conley. 1994. Silicon deposition during the cell cycle of *Thalassiosira weissflogii* (Bacillariophyceae) determined using dual rhodamine 123 and propidium iodide staining. J. Phycol. **30:** 45–55, doi:10.1111/j.0022-3646.1994.00045.x

———, and others. 2011. Co-limitation of diatoms by iron and silicic acid in the equatorial Pacific. Deep-Sea Res. Part II **58:** 493–511, doi:10.1016/j.dsr2.2010.08.005

Bucciarelli, E., P. Pondaven, and G. Sarthou. 2010. Effects of an iron-light co-limitation on the elemental composition (Si, C, N) of the diatoms *Thalassiosira oceanica* and *Ditylum brightwellii*. Biogeosciences **7:** 657–669, doi:10.5194/bg-7-657-2010

Buesseler, K. O. 1998. The decoupling of production and particulate export in the surface ocean. Glob. Biogeochem. Cycles **12:** 297–310, doi:10.1029/97GB03366

Claquin, P., V. Martin-Jézéquel, J. C. Kromkamp, M. J. W. Veldhuis, and G. W. Kraay. 2002. Uncoupling of silicon compared with carbon and nitrogen metabolism and the role of the cell cycle in continuous cultures of *Thalassiosira pseudonana* (Bacillariophyceae) under light, nitrogen, and phosphorus control. J. Phycol. **38:** 922–930, doi:10.1046/j.1529-8817.2002.t01-1-01220.x

Coale, K. H., and others. 2004. Southern Ocean iron enrichment experiment: Carbon cycling in high- and low-Si waters. Science **304:** 408–414, doi:10.1126/science.1089778

Cortese, G., and R. Gersonde. 2007. Morphometric variability in the diatom *Fragilariopsis kerguelensis*: Implications for Southern Ocean paleoceanography. Earth Planet. Sci. Lett. **257:** 526–544, doi:10.1016/j.epsl.2007.03.021

De Baar, H. J. W., and others. 2005. Synthesis of iron fertilization experiments: From the Iron Age in the Age of Enlightenment. J. Geophys. Res. **110:** C09S16, doi:10.1029/2004JC002601

De La Rocha, C. L., D. A. Hutchins, M. A. Brzezinski, and Y. Zhang. 2000. Effects of iron and zinc deficiency on elemental composition and silica production by diatoms. Mar. Ecol. Prog. Ser. **195:** 71–79, doi:10.3354/meps195071

Ebersbach, F., and T. W. Trull. 2008. Sinking particle properties from polyacrylamide gels during the KErguelen Ocean and Plateau compared Study (KEOPS): Zooplankton control of carbon export in an area of persistent natural iron inputs in the Southern Ocean. Limnol. Oceanogr. **53:** 212–224, doi:10.4319/lo.2008.53.1.0212

Franck, V. M., K. W. Bruland, D. A. Hutchins, and M. A. Brzezinski. 2003. Iron and zink effects on silicic acid and nitrate uptake kinetics in three high-nutrient, low-chlorophyll (HNLC) regions. Mar. Ecol. Prog. Ser. **252:** 15–33, doi:10.3354/meps252015

Guillard, R. R. L., and J. H. Ryther. 1962. Studies on marine planktonic diatoms I. *Cyclotella nana* Hustedt and *Detonula confervacea* (Cleve) Gran. Can. J. Microbiol. **8:** 229–239, doi:10.1139/m62-029

Hamm, C. E., R. Merkel, O. Springer, P. Jurkojc, C. Maier, K. Prechtel, and V. Smetacek. 2003. Architecture and material properties of diatom shells provide effective mechanical protection. Nature **421:** 841–843, doi:10.1038/nature01416

Hansen, H. P., and F. Koroleff. 1999. Determination of nutrients, p. 159–228. *In* K. Grasshoff, K. Kremling, and M. Ehrhardt [eds.], Methods of seawater analysis. Wiley-VCH.

Hoffmann, L. J., I. Peeken, and K. Lochte. 2007. Effects of iron on the elemental stoichiometry during EIFEX and in the diatoms *Fragilariopsis kerguelensis* and *Chaetoceros dichaeta*. Biogeosciences **4:** 569–579, doi:10.5194/bg-4-569-2007

———, ———, and ———. 2008. Iron, silicate, and light co-limitation of three Southern Ocean diatom species. Polar Biol. **31:** 1067–1080, doi:10.1007/s00300-008-0448-6

Hutchins, D. A., and K. W. Bruland. 1998. Iron-limited diatom growth and Si : N uptake ratios in a coastal upwelling regime. Nature **393:** 561–564, doi:10.1038/31203

Ianora, A., S. A. Poulet, and A. Miralto. 2003. The effects of diatoms on copepod reproduction: A review. Phycologia **42:** 351–363, doi:10.2216/i0031-8884-42-4-351.1

Jackson, G. A., A. M. Waite, and P. W. Boyd. 2005. Role of algal aggregation in vertical carbon export during SOIREE and in other low biomass environments. Geophys. Res. Lett. **32:** L13607, doi:10.1029/2005GL023180

Jähne, B. 2005. Digital image processing. Springer Verlag.

Kolbowski, J., and U. Schreiber. 1995. Computer-controlled phytoplankton analyzer based on 4-wavelengths PAM chlorophyll fluorometer, p. 825–828. *In* P. Mathis [ed.], Photosynthesis: From light to biosphere. Kluver Academic.

Kruse, S., S. Jansen, S. Krägefsky, and U. Bathmann. 2009. Gut content analyses of three dominant Antarctic copepod species during an induced phytoplankton bloom EIFEX (European iron fertilization experiment). Mar. Ecol. **30:** 301–312, doi:10.1111/j.1439-0485.2009.00284.x

Lam, P. J., and J. K. B. Bishop. 2007. High biomass, low export regimes in the Southern Ocean. Deep-Sea Res. Part II **54:** 601–638, doi:10.1016/j.dsr2.2007.01.013

Leynaert, A., E. Bucciarelli, P. Claquin, R. C. Dugdale, V. Martin-Jézéquel, P. Pondaven, and O. Ragueneau. 2004. Effect of iron deficiency on diatom cell size and silicic acid uptake kinetics. Limnol. Oceanogr. **49:** 1134–1143, doi:10.4319/lo.2004.49.4.1134

Marchetti, A., and N. Cassar. 2009. Diatom elemental and morphological changes in response to iron limitation: A brief review with potential paleoceanographic applications. Geobiology **7:** 419–431, doi:10.1111/j.1472-4669.2009.00207.x

———, and P. J. Harrison. 2007. Coupled changes in the cell morphology and the elemental (C, N, and Si) composition of the pennate diatom Pseudo-nitzschia due to iron deficiency. Limnol. Oceanogr. **52:** 2270–2284, doi:10.4319/lo.2007.52.5.2270

Martin, J. H., and S. E. Fitzwater. 1988. Iron deficiency limits phytoplankton growth in the north-east Pacific subarctic. Nature **331:** 341–343, doi:10.1038/331341a0

———, ———, and R. M. Gordon. 1990. Iron deficiency limits phytoplankton growth in Antarctic waters. Glob. Biogeochem. Cycles **4:** 5–12, doi:10.1029/GB004i001p00005

Martin-Jézéquel, V., M. Hildebrand, and M. A. Brzezinski. 2000. Silicon metabolism in diatoms: Implication for growth. J. Phycol. **36:** 821–840, doi:10.1046/j.1529-8817.2000.00019.x

Michels, J., and S. B. Schnack-Schiel. 2005. Feeding in dominant Antarctic copepods—does the morphology of the mandibular gnathobases relate to diet? Mar. Biol. **146:** 483–495, doi:10.1007/s00227-004-1452-1

Miller, C. B., D. M. Nelson, R. R. L. Guillard, and B. L. Woodward. 1980. Effects of media with low silicic acid concentrations on tooth formation in *Acartia tonsa* Dana (Copepoda, Calanoida). Biol. Bull. **159:** 349–363, doi:10.2307/1541099

Nelson, D. M., P. Tréguer, M. A. Brzezinski, A. Leynaert, and B. Quéguiner. 1995. Production and dissolution of biogenic silica in the ocean: Revised global estimates, comparison with regional data and relationship to biogenic sedimentation. Glob. Biogeochem. Cycles **9:** 359–372, doi:10.1029/95GB01070

Pondaven, P., M. Gallinari, S. Chollet, E. Bucciarelli, G. Sarthou, S. Schultes, and F. Jean. 2007. Grazing-induced changes in cell wall silicification in a marine diatom. Protist **158:** 21–28, doi:10.1016/j.protis.2006.09.002

Rollwagen Bollens, G. C., and M. R. Landry. 2000. Biological response to iron fertilization in the eastern equatorial Pacific (IronEx II). II. Mesozooplankton abundance, biomass, depth distribution and grazing. Mar. Ecol. Prog. Ser. **201:** 43–56, doi:10.3354/meps201043

Russ, J. C. 2002. The image processing handbook, 4th ed. CRC Press.

Saito, H., and others. 2005. Responses of microzooplankton to in situ iron fertilization in the western subarctic Pacific (SEEDS). Prog. Oceanogr. **64:** 223–236, doi:10.1016/j.pocean.2005.02.010

Schmid, A. M., and B. E. Volcani. 1983. Wall morphogenesis in *Coscinodiscus wailesii* Gran and Angst. I. Valve morphology and development of its architecture. J. Phycol. **19:** 387–402, doi:10.1111/j.0022-3646.1983.00387.x

Schultes, S., P. G. Verity, and U. Bathmann. 2006. Copepod grazing during an iron-induced diatom bloom in the Antarctic Circumpolar Current (EisenEx): I. Feeding patterns and grazing impact on prey populations. J. Exp. Mar. Biol. Ecol. **338:** 16–34, doi:10.1016/j.jembe.2006.06.028

Smetacek, V., P. Assmy, and J. Henjes. 2004. The role of grazing in structuring Southern Ocean pelagic ecosystems and biogeochemical cycles. Antarct. Sci. **16:** 541–558, doi:10.1017/S0954102004002317

Takeda, S. 1998. Influence of iron availability on nutrient consumption ratio of diatoms in oceanic waters. Nature **393:** 774–777, doi:10.1038/31674

Timmermans, K. R., B. Van Der Wagt, and H. J. W. De Baar. 2004. Growth rates, half-saturation constants, and silicate, nitrate, and phosphate depletion in relation to iron availability of four large, open-ocean diatoms from the Southern Ocean. Limnol. Oceanogr. **49:** 2141–2151, doi:10.4319/lo.2004.49.6.2141

Turner, J. T. 2002. Zooplankton fecal pellets, marine snow and sinking phytoplankton blooms. Aquat. Microb. Ecol. **27:** 57–102, doi:10.3354/ame027057

Voronina, N. M. 1998. Comparative abundance and distribution of major filter-feeders in the Antarctic pelagic zone. J. Mar. Syst. **17:** 375–390, doi:10.1016/S0924-7963(98)00050-5

Waite, A. M., and S. D. Nodder. 2001. The effect of in situ iron addition on the sinking rates and export flux of Southern Ocean diatoms. Deep-Sea Res. Part II **48:** 2635–2654, doi:10.1016/S0967-0645(01)00012-1

Wassmann, P. 1998. Retention versus export food chains: Processes controlling sinking loss from marine pelagic systems. Hydrobiologia **363:** 29–57, doi:10.1023/A:1003113403096

Zeldis, J. 2001. Mesozooplankton community composition, feeding, and export production during SOIREE. Deep-Sea Res. Part II **48:** 2615–2634, doi:10.1016/S0967-0645(01)00011-X

Associate editor: Robert E. Hecky

Received: 10 October 2010
Accepted: 21 February 2011
Amended: 20 April 2011